Journal of
Computational and Theoretical Nanoscience
Vol. 3, 101–109, 2006

Self-Consistent Solutions of 2D-Poisson and Schrodinger Wave Equations for a Gaussian Doped 50 nm MOSFET

A. Agarwal and S. Dasgupta*

Department of Electronics Engineering, Indian School of Mines, Dhanbad 826004, India

RESEARCH ARTICLE

In this paper a self-consistent solution of two-dimensional Poisson and Schrodinger Wave equation using index formulation method of a 50 nm Gaussian doped Metal-Oxide-Semiconductor-Field-Effect-Transistor (MOSFET) is presented. The MOSFET is assumed to have parabolic source and drain region. It is shown that Quantum Mechanical (QM) effects strongly influence the potential profile and the charge distribution function within the channel of the nano-scale device. These results show that full QM simulations will become mandatory issue for nanoscale MOSFET modeling and design in coming future.

Keywords: Nanoscale MOSFET, Quantum Mechanical Effects, Poisson Equation, Schrodinger Wave Equation, Self Consistent Solution.

1. INTRODUCTION

For the past 30 years, the Integrated Circuit industry has followed a steady path of constantly shrinking device geometry and increasing chip size. This strategy has been driven by the increased performance that smaller device makes possible and increased functionality those larger chips provide. Each new generation has approximately double logic circuit design and increased performance by about 40% while quadrupling the memory capacity.[1] The International Technology Roadmap for Semiconductor (ITRS)[2] now extend the device scaling and functionality scenario to the year 2014 at which point minimum feature size are projected to be 35 nm and chip with more than 10^{11} components are expected to be available. As silicon technology advances, questions about the ultimate performance limits arise. When the channel length of MOSFETs is of the order of 1 μm, the threshold voltage decreases with the decrease in channel length, and breakdown voltage also decreases in the case of an n-channel device. These short channel effects pose many problems in the device design in the development of modern MOSFET.[3]

It is well understood that, as the channel length is reduced, transient effects, such as velocity overshoot, strongly affect the overall electron dynamics within the high electric field and ultra short transit time of the channel. The short transit time becomes comparable with the typical scattering time-scale, of the order of picoseconds. Therefore, scattering mechanisms that are well known to degrade the low-field mobility in "long" channels start losing their efficacy.[4] Because of the extremely small geometry, device simulators must account for and predict phenomenon that often requires the inclusion and understanding of the advanced features. Eventually, as devices are scaled down, transport will pass from the semi classical realm where the particle is relatively "localized" by scattering, to the quantum realm of phase coherent ballistic transport.[5]

Thus to continue miniaturization of circuit elements down to nanometer scale, perhaps even to the molecular scale, it is imperative to bring quantum mechanical effects (QME) in conjunction with conventional classical device equations as predicted by ITRS. Researchers over years have looked upon Quantum Mechanical electron devices (QMEDs) for possible solutions.

To extract information accurately about the charge distribution alone requires the solution of Schrödinger and Poisson equations, assuming QM effects are to be fully accounted for. For most device applications, however 1-D solutions are enough to reveal the critical information and provide necessary corrections to the classical picture. We make use of self-consistent Schrödinger Poisson simulations to examine the validity of several simplifying assumptions made in earlier work. The result should be useful for assessing the performance potential of different

*Author to whom correspondence should be addressed.

 1546-198X/2006/3/101/009 doi:10.1166/jctn.2006.008

transistors designs, for comparing device characteristics against ultimate limits, and for identifying many important technological and theoretical issues for silicon transistors at the end of the roadmap.[6–8]

At the 100-nm technology and beyond, one of the major challenges is to simultaneously meet the requirements the on-and off state currents and to limit the overall chip power dissipation, scaling down both threshold and bias voltage.[9] However, the efficacy of this solution is partly offset by the limitation to the threshold voltage (V_T) scaling imposed by the increase in the offset current due to sub threshold conduction.[10]

It follows that an accurate assessment of device characteristics and performance in the nanoscale range is of fundamental importance to understand the ultimate limits of MOS scaling as well as help to develop innovative device concepts. The investigation of the quantized inversion layer has been initially addressed by one-dimensional (1-D) models that take into account QM effects in the direction normal to the silicon/oxide interface.[11–23] More recently, the impact of quantisation on the drain-current performance of short-channel n- and p-MOSFETs has been deeply investigated employing quasi-two-dimensional (quasi-2-D) QM device simulations.[24–26] In fact, for sub 50 nm MOSFETs the fundamental assumption of homogeneity of the potential well in the plane parallel to the silicon/oxide interface does not hold anymore, even if compared to the electron coherence length, so that a full 2-D treatment of QM effects is required.

In the present paper, we intend to form a self-consistent solution of 2D Poisson and Schrodinger wave equation using index formulation method and obtain the potential profile and electron density probability within the channel region of the nanoscale MOSFET under study.

2. NUMERICAL MODELING

The limitations of analytical method have led the engineers and scientists to evolve graphical and numerical methods. While the graphical results though simple have limitation of giving results with less accuracy, numerical methods have been used to derive results with more accuracy. With the advent of high speed digital computers and increasing demand for numerical answers to various problems, numerical technique have become indispensable tool in hand of engineers.

Numerical methods are often, of a repetitive nature. These consist repeated execution of the same process where at each step the results of the preceding step is used. This is known as iteration process and is repeated till the result is obtained to a desired degree of accuracy.

The longitudinal direction has been chosen as the x-axis of the device and the lateral direction from Si–SiO_2 interface into the substrate is treated as y-axis. Infinite source junction depth was assumed in previous works in order to simplify mathematical derivations. However this overestimates the short channel effects of MOSFETs. In order to aid in solution by numerical method a three line approximation has been made to the parabolic model.

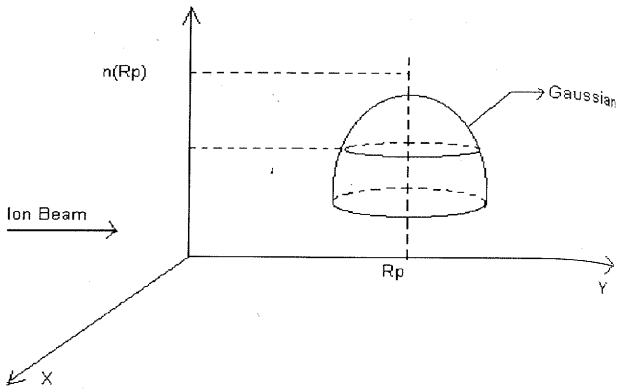

Fig. 1. Gaussian dopant distribution showing the various axes.

The lateral motion of the ions leads to a lateral Gaussian distribution shown in Figure 1 with standard deviation. We can write the ion concentration as

$$N_a(y) = n_0 \exp[-(y - R_p)^2/2\sigma_p^2] \quad (1)$$

Where, n_0 is the concentration at the Si–SiO_2 interface, $N_a(y)$ is the space dependent Gaussian concentration profile of the dopant, R_p is the projected range and σ_p is the straggle parameter associated with the gaussian profile of the introduced dopant.

To extract information accurately about the charge distribution alone requires the solution of Schrödinger and Poisson equations, assuming QM effects are to be fully accounted for Self-consistent Schrödinger Poisson simulations is believed to be the most accurate approach to simulate carrier transport in deep sub micrometer region, where non-stationary transport and high electric fields dominate the device properties. To determine the different eigenstates and eigen values of potential within the channel two dimensional Poisson equations as well as Schrödinger equation are solved. For very small channel length in nanometer-scale, Quantum Mechanical effects comes in picture and their effects are included by solving Schrödinger equation in succession with Poisson equation i.e., by self consistent solution of Poisson and Schrödinger equation.

Considering the two dimensional Poisson's equation in a rectangular coordinate system, the second–order elliptical differential equation for the potential distribution in an n-channel MOS structure can be written as,

$$\nabla^2\Phi(x, y) = \frac{q}{\varepsilon_{si}} N_a(y) \quad (2)$$

where Φ is the electrostatic potential, q is the electronic charge and $N_a(y)$ is space dependent acceptor ion concentration.

This equation is solved for rectangular substrate along its length and depth. The boundary conditions applied to solve two-dimensional Poisson's Equation are

$$\Phi(x,0) - t_{ox}\frac{\varepsilon_{si}}{\varepsilon_{ox}}\left.\frac{\partial\Phi}{\partial y}\right|_{y=0} = V_G - V_{FB} \tag{3a}$$

$$\Phi(0,y) = \Phi_{bi} \tag{3b}$$

$$\Phi(L,y) = \Phi_{bi} + V_D \tag{3c}$$

$$\left.\frac{\partial\Phi}{\partial y}\right|_{y=W_d} = 0 \tag{3d}$$

where V_{fb} is the flat-band voltage, t_{ox} is the oxide thickness, ε_{ox} is the permittivity of the oxide layer, Φ_{bi} is the built in voltage and W_d is the width of the depletion region in the substrate. Equation (3) implies that the gate voltage (i.e., $V_G - V_{FB}$) is the sum of the surface potential ($\Phi(x,0)$) and the voltage drop due to y-component of the electric field. ($E_Y = -\partial\Phi/\partial y$) is the electric field along lateral direction from Si–SiO_2 interface towards substrate.

Different eigen values can be found in the channel region by solving the Poisson equation

$$-\nabla(\varepsilon\nabla\Phi) = \rho_{cl} + \rho_q \tag{4}$$

Where, ρ_{cl} is the classical charge in the channel region of the nano-MOSFET given by

$$\rho_{cl} = n_{po}\exp(-\beta\Phi(x,y)) \tag{5}$$

Here n_{po} is the electron charge concentration at equilibrium, Φ is the electrostatic potential, $\beta = q/kT$ where T is the operating temperature, k is the Boltzmann constant and q is the electronic charge.

The quantum charge used in Eq. (4) is defined as[18]

$$\rho_q = -e\sum_{n=0}^{+\infty} A_D|\Psi_n|^2 F_y\left(\frac{(E_f - E_n)}{K_B T}\right) \tag{6}$$

where A_D is the coefficient depending on dimensionality, E_f is the Fermi level, E_n are the eigen energies corresponding to ψ_n eigen values and F_y is the generic Fermi-Dirac integral, of order 0 for quantum- well problems, order $-1/2$ for quantum wires. For efficient solution of the above equation in the nanometric region, Schrödinger equation and Poisson equation are solved in succession. Schrödinger wave equation is given by

$$\frac{\hbar^2}{2}\nabla\left(\frac{\nabla\psi_n}{m^*}\right) + E_c\psi_n = E_n\psi_n \tag{7}$$

where

$$E_c = -e\Phi + \Delta E_c \tag{8}$$

m^* is the effective mass of electron taken as 0.95 m_0, m_0 being the rest mass of the electron in the channel, ψ_n are the electron eigen states, E_c is the potential energy and ΔE_c is material dependant offset. To solve Poisson's and Schrödinger's equation, classical five point discretization methods are used in which whole substrate is divided into number of columns and rows.

Using classical five point discretization method, the Poisson equation reduces to

$$-\varepsilon\left(\frac{(\phi_{i+1,j}-\phi_{i,j})/h_i - (\phi_{i,j}-\phi_{i-1,j})/h_{i-1}}{(h_i+h_{i-1})/2} + \frac{(\phi_{i,j+1}-\phi_{i,j})/k_j - (\phi_{i,j}-\phi_{i,j-1})/k_{j-1}}{(k_j+k_{j-1})/2}\right) = \rho_{cl} + \rho_q \tag{9}$$

Assuming $h_I = k_j$ and solving equation 9, we get

$$\Phi_{ij} = \frac{1}{4}\left(\Phi_{i,j-1} + \Phi_{i,j+1} + \Phi_{i-1,j} + \Phi_{i+1,j} - \rho\frac{h^2}{\varepsilon_{si}}\right) \tag{10}$$

Thus $\Phi_{i,j}$ can be found by solving Eq. (10) iteratively and using given boundary conditions (Eq. 3(a)–3(d)).

The two dimensional Schrödinger equation is

$$-\frac{\hbar^2}{2m^*}\left(\frac{\partial^2}{\partial x^2} + \frac{\partial^2}{\partial y^2}\right)\psi(x,y) + V(x,y)\psi(x,y) = E\psi(x,y) \tag{11}$$

Consider a system with finite spatial resolution. For the sake of simplicity, let us say ψ is only interesting (non-zero) in the square Cartesian domain $[x|-a<x<a],[y|-a<y<a]$. To make ψ into a matrix, we choose a spatial resolution for x and y. In this case we choose N_x and N_y so that $\psi(x,y)$ and $V(x,y)$ are N_x by N_y matrices. Then the spatial resolution will be given by $\delta x = 2a/N_x$ and $\delta y = 2a/N_y$. For the purpose of this problem, we assume $N_x = N_y = N$, implying $\delta x = \delta y$. This makes V and ψ square $N \times N$ matrices. More conveniently ψ can be written as

$$\overline{\psi} = \left(\psi_{1,1}\psi_{2,1}\cdots\psi_{N,1}\psi_{1,2}\psi_{2,2}\cdots\psi_{N,2}\cdots\psi_{N,N}\right)^T \tag{12}$$

Where we have used the notation $\psi_{n,m} \equiv \psi(x_n, y_m)$. Using the same notation equation (11) take the discrete form

$$\frac{d^2}{dx^2}\psi_{n,m} = \frac{\psi_{n+1,m} - 2\psi_{n,m} + \psi_{n-1,m}}{\delta x^2} \tag{13}$$

And the discrete two-dimensional Schrodinger equation is

$$-\frac{\hbar^2}{2m^*}\left(\frac{\Psi_{n+1,m} - 2\Psi_{n,m} + \Psi_{n-1,m}}{\delta x^2} + \frac{\Psi_{n,m+1} - 2\Psi_{n,m} + \Psi_{n,m-1}}{\delta y^2}\right) + V_{n,m}\Psi_{n,m} = E\Psi_{n,m} \tag{14}$$

if $\delta x = \delta y$, the above reduces to

$$-\frac{\hbar^2}{2m^*\delta x^2}(\Psi_{n+1,m} + \Psi_{n-1,m} + \Psi_{n,m-1} - 4\Psi_{n,m}) + V_{n,m}\psi_{n,m} = E\psi_{n,m} \tag{15}$$

It is convenient to have energy and potential represented as dimensionless functions, therefore, defining new variables

$$U_{n,m} = \frac{V_{n,m}}{E_o} - 4 \equiv -\frac{8ma^2}{N^2\hbar^2}V_{n,m} - 4 \tag{16}$$

$$\lambda = \frac{E}{E_o} \equiv -\frac{8ma^2}{N^2\hbar^2}E \tag{17}$$

Where, $U_{n,m}$ is the dimensionless potential, λ is the eigenvalue or dimensionless energy and the constant E_0 is defined as

$$E_0 = -\frac{N^2\hbar^2}{8ma^2} \tag{18}$$

Thus the Hamiltonian takes a convenient form as

$$\Psi_{n+1,m} + \Psi_{n-1,m} + \Psi_{n,m-1} + \Psi_{n,m+1} - 4\Psi_{n,m} + U_{n,m}\Psi_{n,m} = \lambda\Psi_{n,m} \tag{19}$$

If we write both ψ and U in the vector form, then we can write the Schrödinger equation as a matrix eigenvalue problem in the form $H\psi = \lambda\psi$ where H is the Hamiltonian.

From above matrix we solve for eigen values λ and then solve Eq. (19) to get the value of ψ.

3. RESULTS AND DISCUSSION

The various parameters used in modeling of nanometric MOSFET are shown in Table I. The modeling has been carried out at 300 K. The simulations and the modeling for the device were carried out in a Pentium-II system using MATLAB 5.0 platform in a WINDOWS environment.

Figures 2 and 3 shows the variation in dopant concentration along the substrate lateral direction when Gaussian function of the dopant is taken into consideration in the non-uniforms concentration term of Eq. (1). The two figures show the change in the concentration profile when the range and the straggle parameters are changed. Figure 2 shows the concentration profile for dose-ion range of 20-nm and straggle parameter of 3-nm and Figure 3 shows the concentration profile for dose-ion range of 35-nm and straggle parameter of 7 nm. From these figures it is evident that increasing the range of dopant, shifts the position of the peak of Gaussian profile away from Si–SiO_2 interface into the substrate. This is due to the fact as the range is enhanced there is a larger probability for the dopant to place themselves deeper into the substrate as is seen from the above figures. With an increase in the straggle parameter as is seen from Figure 2 and Figure 3, the bell structure of Gaussian profile increases in width, although the peak value and its position relative to gate end remains constant. This implies that the dopant is more

Table I. Parameters used for modelling.

Parameter	Value
L	50 nm
W	140 nm
ε_{si}	$11.2 * \varepsilon_o$
N_i	1.45e16;
N_a	4.6e20;
q	1.6e–19
k	1.38e–23
m^*	$0.95 * m_o$

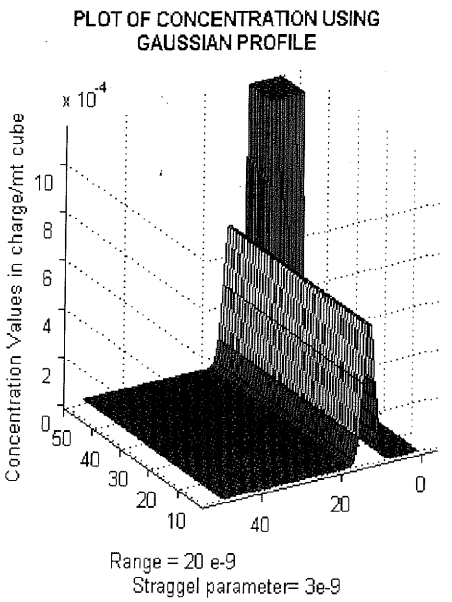

Fig. 2. Dopant concentration variation in the device for the range of 20 nm and straggle parameter of 3 nm.

spread out in the substrate in the case of higher straggle parameter. Also, as it can be seen from Figure 2, the concentration of drain is uniform and double of that of maximum substrate concentration. Although this is case for source also, but here we have shown for drain only to facilitate viewing of variation of Gaussian concentration in substrate more clearly.

Figure 4 shows a three-dimensional view of initial potential distribution. The x-axis in the figure shows the longitudinal direction, the y-axis indicates the lateral direction from the Si/SiO_2 interface and the z-axis shows the potential of the charge carrier in the bulk, which includes

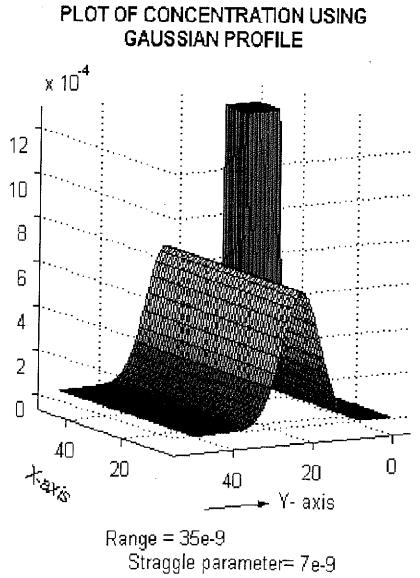

Fig. 3. Dopant concentration variation in the device for the range of 35 nm and straggle parameter of 7 nm.

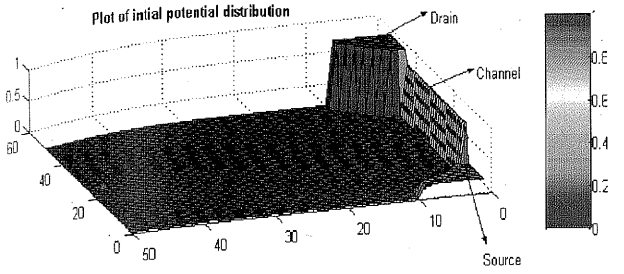

Fig. 4. Initial 2D potential distribution of the device for source, drain and gate voltage of 0.2 V, 1.0 V, and 0.8 V respectively.

the channel and the substrate of the device. The source voltage is 0.2 V and the drain end voltage is 0.8 V as is evident from the boundary conditions imposed on the device. The effective applied effective gate voltage is 0.8 V. The potential proceeds from a lower to a higher value in the channel as one moves from the source end of the gate to the drain end of the gate. Due to sudden increase in potential at the source diffusion junction, a high electric filed is present which forces the electron to travel to the channel region towards the drain end. As we move from the $Si–SiO_2$ interface it can be seen that the potential falls to zero exceedingly fast. This is due to the fact that the lateral electric field is zero at the edge of the depletion region of the nano-MOSFET.

Figure 5 gives a three-dimensional view of the potential distribution obtained after solving the Poisson's equation. The voltage at drain and source end is kept constant. This

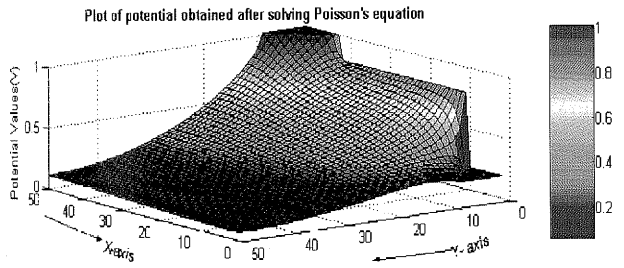

Fig. 5. Final 2D potential distribution of the device obtained after solving the 2D Poisson's equation for source, drain and gate voltage of 0.2 V, 1.0 V, and 0.8 V respectively.

is because perfect conductivity has been assumed in this region. In lateral direction, the voltage goes on increasing from source to drain. The sudden increase in voltage at source junction leads to the formation of very high electric field, which attracts electrons from substrate to form a conducting channel. The voltage in lateral direction goes on decreasing with voltages finally attaining a zero value at certain distance from the gate end. This is because the body of substrate is grounded. Due to this gradual decrease in lateral direction, the lateral electric field is less than longitudinal field resulting in net force on electron in longitudinal direction thereby, their movement from source to drain.

Figures 6 and 7 show the potential distribution in substrate obtained by solving Poisson's equation for different values of gate voltage and same drain voltage and source voltage. The source voltage (V_s) and drain voltage (V_d) is taken to be 0.2 V to be 1.0 V respectively. In Figure 6, where gate voltage is zero, a zero potential is present in channel region, thus no electric field is present here and no channel is formed in this case. However near the drain end where effective gate voltage is V_G-V_d, a small potential is present around drain junction. Thus for zero gate voltage we get zero drain current, although drain voltages may be considerable higher. In Figure 7, the gate voltage is increased to a value of 0.5 V. It can be seen from the figure that the potential distributes itself in channel region and thus an electric field in the longitudinal direction is now present. This electric field attracts the electron so as to form the channel necessary for conduction process. As we go on increasing the gate voltage, the potential values in the channel also go on increasing. Also, the potential distribution attains non-zero values along the depth at a greater distance for more gate voltage. This is because; now higher electrons are being attracted to form the conduction channel. In Figure 7, the distribution shown is for ideal drain current. A further increase in gate voltage from these values only increases the potential values and thereby higher electric field but does not have much effect on the drain current.

Figures 8 and 9 show the potential distribution in substrate obtained by solving Poisson's equation for different

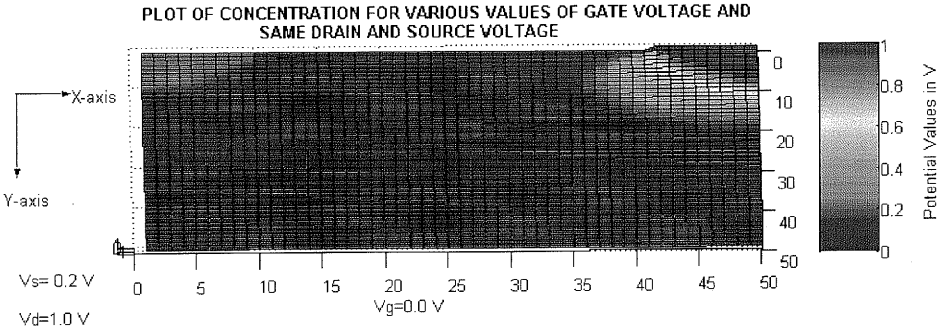

Fig. 6. Final 2D potential distribution of the device obtained after solving the 2D Poisson's equation for source, drain and gate voltage of 0.2 V, 1.0 V, and 0.0 V respectively.

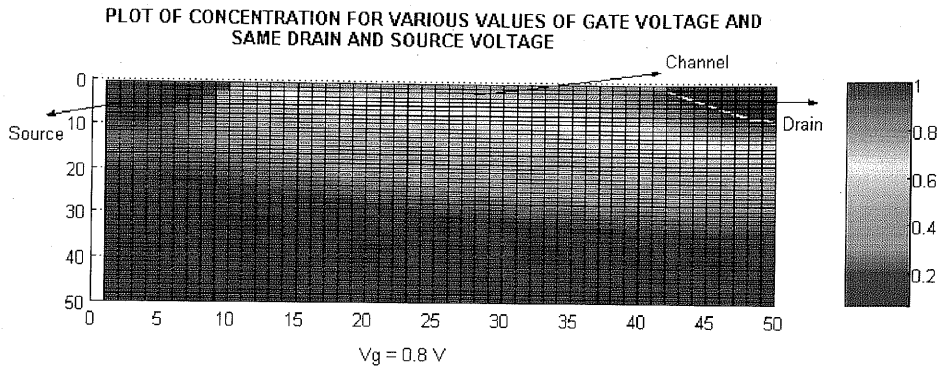

Fig. 7. Final 2D potential distribution of the device obtained after solving the 2D Poisson's equation for source, drain, and gate voltage of 0.2 V, 1.0 V, and 0.8 V respectively.

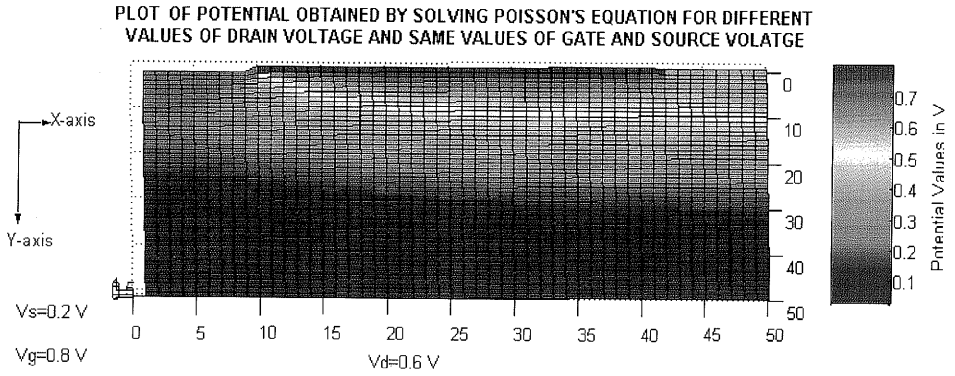

Fig. 8. Final 2D potential distribution of the device obtained after solving the 2D Poisson's equation for source, drain, and gate voltage of 0.2 V, 0.6 V, and 0.8 V respectively.

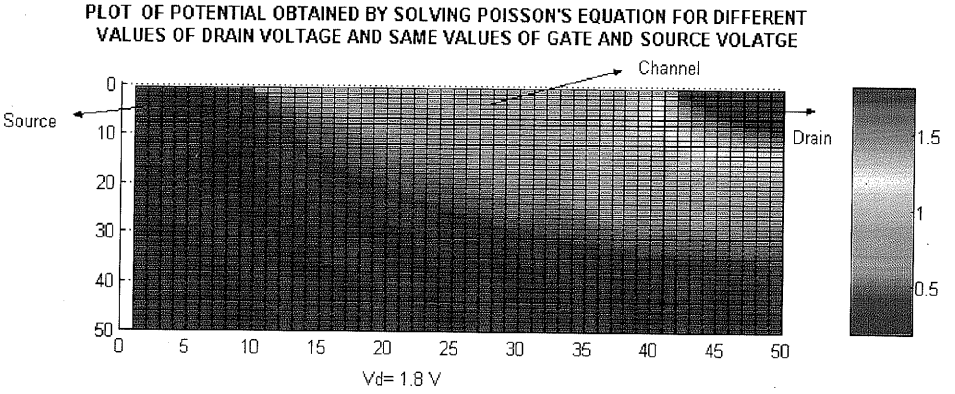

Fig. 9. Final 2D potential distribution of the device obtained after solving the 2D Poisson's equation for source, drain, and gate voltage of 0.2 V, 1.8 V, and 0.8 V respectively.

values of drain voltage and same gate voltage and source voltage. The source voltage has been taken to 0.2 V and gate voltage to be 0.8 V. It can be seen from Figure 8, that for low drain voltages, potential distribution in channel is mainly dependant on gate voltage and if this gate voltage is greater than the pinch off voltage, a conduction channel is formed. However for low values of drain voltages, small electric field is present near the drain end resulting in less carrier concentration at drain end. In Figure 9, as we increase the drain voltage values, the potential in lateral direction attains non-zero values for greater distance and also, high electric field at drain now leads to large accumulation of carriers near drain end.

Figures 10 to 11 show the plot of eigen values with varying index values of eigen values of the Hamilton matrix for various drain voltage and same gate and source voltage. The source voltage has been taken to be 0.2 V, and gate voltage has been taken to be 0.8 V. Figure 10 shows the variation of eigen values for a drain voltage of 0.6 V. The index values vary from 0–2500. As can be seen from

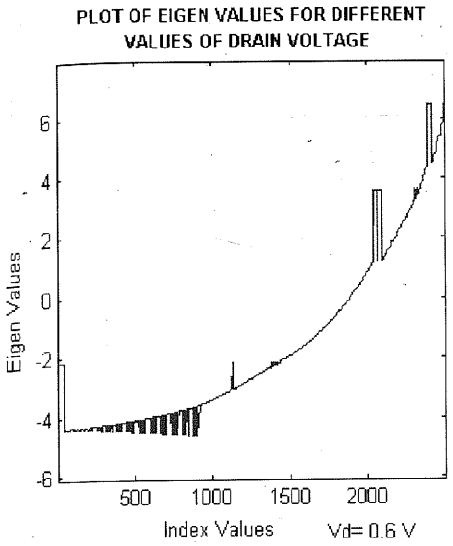

Fig. 10. Plot of eigen values Vs index value for source, drain, and gate voltage of 0.2 V, 0.6 V, and 0.8 V respectively.

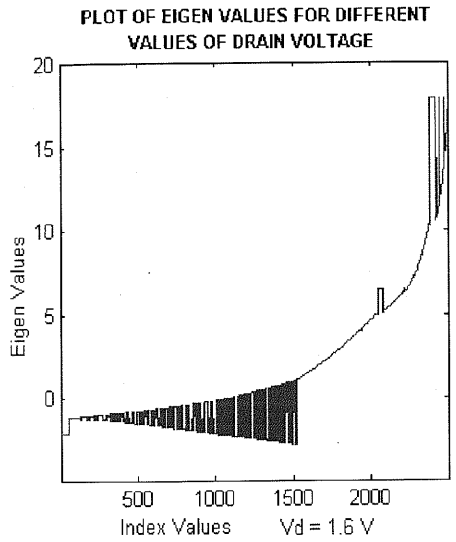

Fig. 11. Plot of eigen values Vs index value for source, drain, and gate voltage of 0.2 V, 1.6 V, and 0.8 V respectively.

figure the eigen values shows perturbation and oscillations near lower index values and few of these near higher index values. For higher drain voltage it can be shown that the oscillations tends to increase and their values also tends to increase, as is evident from Figure 11. This is due to the fact that at higher drain voltage, the longitudinal electric field near the drain end as well as near the source end increases, which results in a higher energy level in the conduction band. This is known as Hot Carrier Effects.

Figures 12 to 15 show the variation in the electron concentration in the substrate when the Schrodinger solution is obtained for one eigen value chosen from the many eigen values of the Hamilton matrix given in Eq. (19). These variations have been obtained for different values of drain voltages and same value of applied gate and source voltage. Source voltage has been taken to be 0.2 V and gate voltage to be 0.8 V. In the figure, the x-axis is the lateral direction from source to drain end and y-axis denotes the relative value of the electron concentration. It can be seen from the figure as the drain voltage is increased the electron concentration increases. Also the width of the profile also increases or in other word there is a lateral displacement of the electron concentration along the channel length. As the drain voltage increases the effective channel potential increases, which results in larger concentration. For an applied drain voltage of 1.6 V there is a presence of double hump in the electron concentration which might be due to effective quantisation of the electron along the channel length at such high applied voltages.

Figures 16 and 17 show the potential plot obtained by solving the Poisson's and Schrödinger equation in a self-consistent manner. These plots have been obtained for source voltage equal to 0.2 V, gate voltage equal to 0.8 V, and drain voltage equal to 1.0 V. The solution of Schrödinger equation, square of which gives the probability to find an electron, gives a hump near the drain end. This is due to the presence of high electric field at the drain end that leads to the accumulation of electrons near the drain end.

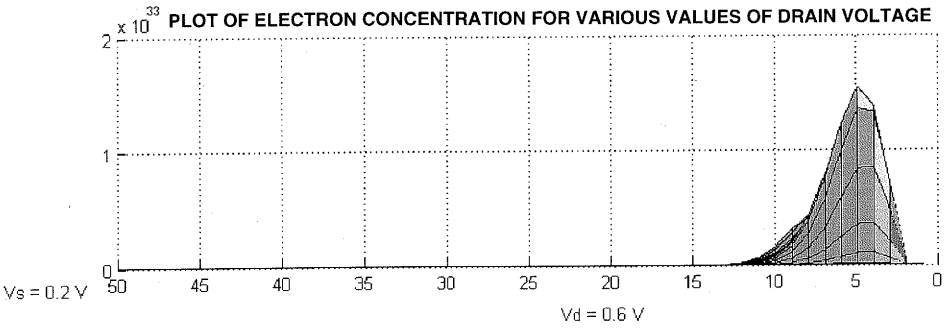

Fig. 12. Plot of electrons concentration in substrate obtained after solving the Schrodinger equation for source, drain, and gate voltage of 0.2 V, 0.6 V, and 0.8 V respectively.

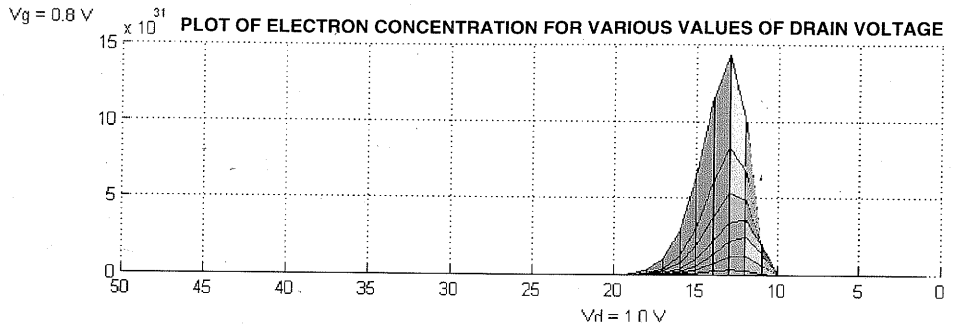

Fig. 13. Plot of electrons concentration in substrate obtained after solving the Schrodinger equation for source, drain, and gate voltage of 0.2 V, 1.0 V, and 0.8 V respectively.

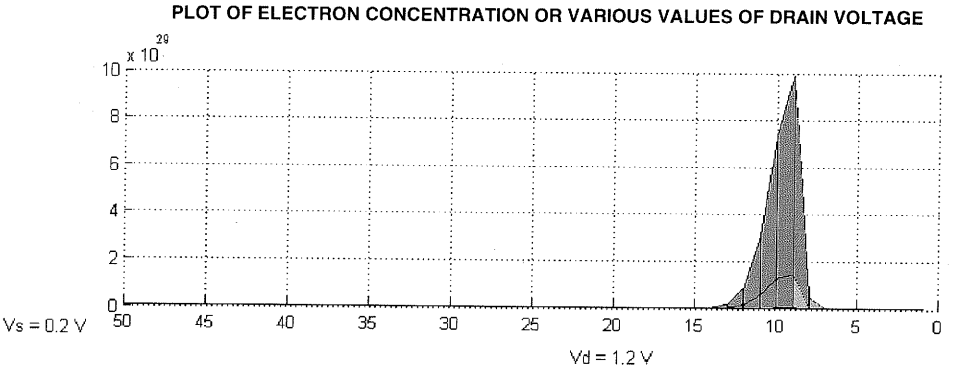

Fig. 14. Plot of electrons concentration in substrate obtained after solving the Schrodinger equation for source, drain, and gate voltage of 0.2 V, 1.2 V, and 0.8 V respectively.

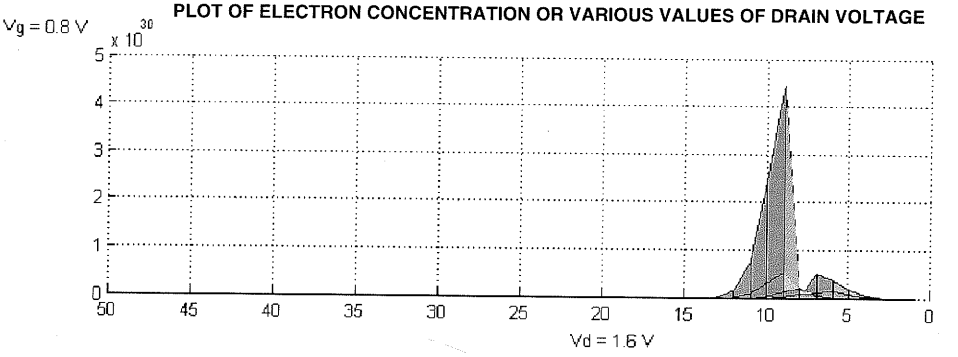

Fig. 15. Plot of electrons concentration in substrate obtained after solving the Schrodinger equation for source, drain, and gate voltage of 0.2 V, 1.6 V, and 0.8 V respectively.

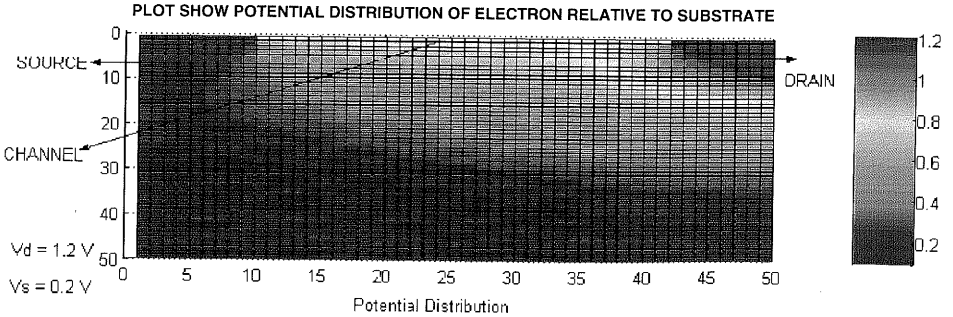

Fig. 16. Final potential distribution of the device obtained after solving the 2D Poisson's equation for source, drain, and gate voltage of 0.2 V, 1.0 V, and 0.8 V respectively.

RESEARCH ARTICLE

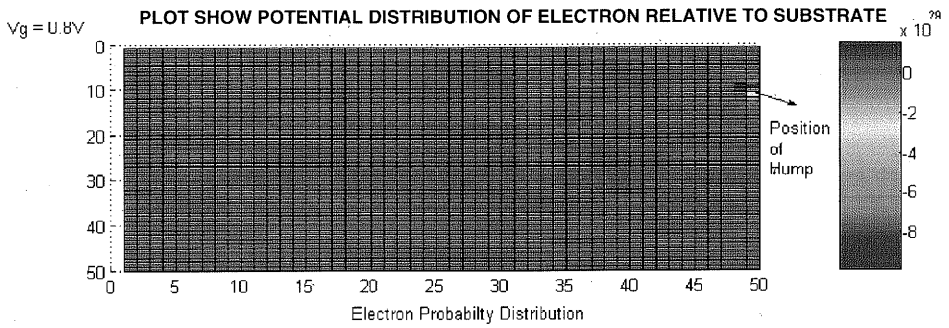

0.2 V, 1.0 V,

Fig. 17. Plot showing position of hump representing probability to find electrons in substrate relative to substrate obtained after solving the Schrodinger equation for source, drain, and gate voltage of 0.2 V, 0.6 V, and 0.8 V respectively.

4. CONCLUSION

The present work attempts to find the profiling of the channel of a Gaussian doped nano-meter MOSFET. It also attempts to find out the three dimensional potential distribution across the channel taking into consideration the QM effects. The Hamilton matrix has been solved to get the Eigen values for the various drain and gate voltages. This in turn gives the knowledge of electron concentration within the channel. The present work will find use in modeling and simulation of future nano-MOSFETs for their ultimate assimilation onto a ULSI scheme. It will also find use for the device engineers and fabricators to simulate the device on a platform before going into actual fabrication process, which would result in the semiconductor fabrication industry.

0.2 V, 1.2 V,

Acknowledgment: One of the authors (SDG) would like to acknowledge the financial support give by MHRD, GOI under thrust area scheme. (No.F-27-3/2002TS.V).

References

1. J. D. Plummer and P. B. Griffin, *Proc. IEEE* 89, 240 (**2001**).
2. Semiconductor Industry Association, International Technology Roadmap for Semiconductor (**2001**).
3. Toru Toyabe and Shojiro Asai, *IEEE Trans. on Electron Devices* 26, 453 (**1979**).
4. Wanqiang Chen, Leonard F. Register, and Sanjay K. Banerjee, *IEEE Trans. on Electron Devices* 49, 652 (**2002**).
5. Gabriele F. Formicone and Marco Saraniti, *IEEE Trans. on Electron Devices* (**2002**).
6. *National Technology Roadmap for Semiconductors*, Semiconductor Industry Association (**2000**).
7. Farzin Assad, Zhibin Ren, Dragica Vasileska, Supriyo Datta, and Mark Lundstrom, *IEEE Trans. on Electron Devices* 47, 232 (**2000**).
8. W. Kohn and L. J. Sham, *Phys. Rev.* 140, 1067 (**1982**).
9. *International Technological Roadmap for Semiconductors*, Semiconductor Industry Association, San Jose, CA (**1999**).
10. Y. Taur, C. H. wann, and D. J. Frank, *IEDM Tech. Dig.* 789 (**1998**).
11. C. Moglestue, *J. Appl. Phys.* 59, 3175 (**1986**).
12. Y. Ohkura, *Solid-State Electron.* 33, 1581 (**1990**).
13. S. Imanaga and Y. Hayafuji, *J. Appl. Phys.* 70, 1522 (**1991**).
14. J. Suñé, P. Olivo, and B. Riccò, *J. Appl. Phys.* 70, 337 (**1991**).
15. C. Jungemann, A. Emunds, and W. L. Engl, *Solid-State Electron* 36, 1529 (**1993**).
16. T. Janik and B. Majkusiak, *J. Appl. Phys.* 75, 5186 (**1994**).
17. C.-Y. Hu, S. Banerjee, K. Sadra, B. G. Streetman, and R. Sivan, *IEEE Electron Device Lett.* 17, 276 (**1996**).
18. A. Pacelli, *IEEE Trans. on Electron Devices* 44, 1169 (**1997**).
19. J. A. Lopez-Villanueva, P. Cartujo-Casinello, J. Banqueri, F. Gamiz, and S. Rodriguez, *IEEE Trans. on Electron Devices* 44, 1915 (**1997**).
20. S. Jallepalli, J. Bude, W.-K. Shih, M. R. Pinto, C. M. Maziar, and A. F. Tasch, *IEEE Trans. Electron Devices* 44, 297 (**1997**).
21. D. Vasileska and D. K. Ferry, *IEEE Trans. Electron Devices* 44, 577 (**1997**).
22. D. Vasileska, D. K. Schroder, and D. K. Ferry, *IEEE Trans. Electron Devices* 44, 584 (**1997**).
23. N. Yang, W. K. Henson, J. R. Hauser, and J. J. Wortman, *IEEE Trans. Electron Devices* 46, 1464 (**1999**).
24. A. Spinelli, A. Benvenuti, and A. Pacelli, *IEEE Trans. Electron Devices* 45, 1342 (**1998**).
25. A. S. Spinelli, A. Benvenuti, S. Villa, and A. L. Lacaita, *IEEE Electron Device Lett.* 20, 298 (**1999**).
26. A. S. Spinelli, A. Benvenuti, L. Conserva, A. L. Lacaita, and A. Pacelli, *Proc. SISPAD* 192 (**2000**).

Received: 5 May 2005. Accepted: 31 May 2005.